Flat and Spherically Bent Muscovite (Mica) Crystals for X-ray Spectroscopy

Physica Scripta. Vol. 57, 301–309, 1998

Flat and Spherically Bent Muscovite (Mica) Crystals for X-ray Spectroscopy

G. Hölzer,*[1] O. Wehrhan,[1] J. Heinisch,†[1] E. Förster,[1] T. A. Pikuz,[2] A. Ya. Faenov,[2] S. A. Pikuz,[3] V. M. Romanova[3] and T. A. Shelkovenko[3]

[1] X-ray optics group, Institute for Optics and Quantum Electronics, Friedrich-Schiller-University Jena, D-07743 Jena, Germany
[2] Multicharged Ions Spectra DataCenter, VNIIFTRI, Mendeleevo, Moscow region, 141570, Russia
[3] P. N. Lebedev Physical Institute, Leninskii prospekt 53, Moscow, Russia

Received May 27, 1997; accepted June 9, 1997

PACS Ref: 61.10-i, 61.50Ah, 52.25Nr

Abstract

Essential parameters for the application of crystals to quantitative X-ray spectroscopy are the upper wavelength limit and the quantitative reflection properties (intrinsic resolving power, luminosity) of the crystal. Due to the large lattice constant, muscovite, a mica group mineral, can be used in the wavelength range up to about 2 nm. Muscovite crystals can be bent to small radii of curvature due to their favourable cleavage and elastic properties. Characteristic reflection properties at reflections 002 – 00 24 were investigated theoretically and experimentally. The integrated reflectivity was calculated for various reflections of perfect flat as well as spherically bent muscovite crystals with curvature radii $R = 100$ and $R = 186$ mm. It was measured for flat crystals in the reflections 00 10 – 00 26 using CuKα- and MoKα-radiation from X-ray tubes and compared with calculations for both perfect and mosaic crystals. Available high-quality muscovite crystals have a mosaic structure with a mosaic spread of about 1 arcmin. This mosaic spread limits the spectral resolving power for high reflection orders.

1. Introduction

Crystals are frequently used as dispersive elements in laser plasma diagnostics, high resolution X-ray spectroscopy and X-ray astronomy (see for example [1]). Flat crystals with narrow reflection curves can be used in a broad spectral range and provide a high spectral resolving power. The luminosity is small due to the small angular aperture. The spatial resolution is usually limited by the source size. For spectroscopy with extended sources, the spatial resolution and the luminosity of the spectrometer can be improved considerably by using focusing geometries with one- or two-dimensionally bent crystals. An important factor which determines the performance of spectrometers with bent crystals are aberrations characteristic for the selected geometry [2–4]. Further the bending of a crystal will cause characteristic changes of the intrinsic reflection properties of the crystal itself. In the Bragg case a long exponentionally decreasing tail appears in the reflection curve of a bent crystal [5]. For smaller radii of curvature the integrated reflectivity and consequently the luminosity of the spectrometer increases from the dynamical (perfect crystal) to the larger kinematical (mosaic crystal) limit. However the resolving power decreases due to the broadening of the reflection curve.

The successful application of flat and bent crystals for X-ray spectroscopy requires highly developed techniques for crystal preparation and bending, precise test methods for the crystal quality and a good quantitative knowledge of the crystal reflection properties for a quantitative analysis of the recorded spectra. Spectrometers with flat, one- and two-dimensionally bent crystals of silicon, germanium, quartz, ADP, KAP, RAP, TlAP, PET and LiF were prepared by the Jena group and successfully applied in plasma diagnostic experiments (see for example [6, 7]) and high resolution X-ray spectroscopy [8]. The real structure (crystal perfection) and the reflection properties of flat and bent crystals were tested by X-ray topography, measurements of the integrated reflectivity and imaging tests for two-dimensionally bent crystals [6]. The reflection properties of perfect flat and elastically bent crystals are calculated using the dynamical theory of X-ray diffraction [9].

For X-ray spectroscopy in the wavelength range above 1 nm only a few crystals are available. Mica crystals allow the spectral range to be extended to about 2 nm due to their large lattice constant of about 2 nm [10]. Thin crystals are easily produced by cleavage. The small thickness and the elastic properties are favourable for bending to small radii of curvature. Spherically bent crystals with such small radii ($R \leqslant 100$ mm) and a large working area of $8 \times 26\,\text{mm}^2$ are available. But mica crystals have a mosaic structure and a preselection of highly perfect crystals is essential for their application in high-resolution spectroscopy. This is one reason why an analysis of the reflection properties of mica is very desirable. We present a detailed theoretical and experimental study of the structural and reflection properties of flat and spherically bent mica crystals. In Chap. 2 the characteristic intrinsic reflection properties of flat and spherically bent crystals are discussed taking into account the mosaic structure. The study is intentionally limited to the reflection properties of muscovite: measurements of the integrated reflectivity (Chap. 3), topographic studies of flat and bent crystals (Chap. 4) and imaging tests with bent crystals (Chap. 5).

* email: ghoelzer@roentgen.physik.uni-jena.de
† Now at Trioptics GmbH, D-22880 Wedel, Germany

2. Reflection properties of muscovite

The structure and the chemical composition of the analyzed crystals was determined by a chemical analysis as muscovite, a mica group mineral. Structure data from Güven [10] were used for the calculation of the X-ray reflection properties. The data had to be slightly simplified for the calculation, a partial substitution of 25% of the Si-atoms by Al in the tetrahedron structures cannot be taken into account. The effect of this simplification is small because Al (atomic number 13) and Si (atomic number 14) are neighbours in periodic system and have nearly the same scattering characteristics.

The X-ray reflection curves of flat and bent muscovite crystals in the Bragg case were computed using the dynamical theory of X-ray diffraction (see for example [11, 9]). For bent crystals the Takagi–Taupin theory [9] is used. The reflection curve $R(y) = XX^*$ of a "thick" (thickness $\gg$ penetration depth of the X-rays) elastically bent crystal in the Bragg case can be determined by solving the differential equation

$$\mathrm{i}C\,\frac{\mathrm{d}X}{\mathrm{d}y} = X^2(1 + \mathrm{i}\kappa) - 2X(y + \mathrm{i}g) + (1 + \mathrm{i}\kappa). \tag{1}$$

X is the complex amplitude of the diffracted radiation at the crystal surface (the amplitude of the incoming radiation is normalized to unity), y is the normalized angular variable of the reflection curve, g and κ represent the absorption of the incoming and the scattered radiation, respectively. For a detailed description of the notations we refer to [9]. C introduces the crystal deformation due to the elastic bending (considering here only the symmetrical diffraction case):

$$C = \frac{2\lambda \cdot \sin\theta_\mathrm{B}}{\pi(\chi_h \chi_{\bar{h}})} \times \left[\frac{1}{R_x} \cdot \cos^2\theta_\mathrm{B} - \left(\frac{1}{R_x} + \frac{1}{R_y}\right) \cdot \frac{\sigma}{1-\sigma} \cdot \sin^2\theta_\mathrm{B}\right]. \tag{2}$$

R_x and R_y are the curvature radii in and perpendicular to the diffraction plane, θ_B is the Bragg angle, χ_h and $\chi_{\bar{h}}$ are the Fourier components of the electric susceptibility, λ is the X-ray wavelength and σ is the Poisson ratio. The first term in eq. (2) takes into account the pure geometrical bending, the second one the change of the lattice plane distance due to bending and depends on the elastic properties of the crystal. The anisotropic elastic constants of muscovite in a monoclinic quasi-hexagonal approximation can be found in [12] for the reference system of crystal physics and have to be transformed to the coordinate system of the specimen. For the surface orientation (001) σ is equal to 0.217. This value is constant for any position of the bending axis inside the surface generated by a rotation around the surface normal [001]. Incoming unpolarized radiation is assumed. The crystal reflection data are calculated using the computer code DIXI developed by one of the authors (G.H.).

To test the structure model calculated reflection parameters (integrated reflectivity R_int, peak reflectivity P and full width at half maximum FWHM $\Delta\theta_\mathrm{cp}$ of the reflection curves) of flat perfect muscovite crystals in the reflection 002 are compared with published data of Henke *et al.* [13]. The agreement is better than 1% for the FWHM $\Delta\theta_\mathrm{cp}$ and peak reflectivity P. Our data of R_int for the dynamical and the mosaic crystal limits are generally smaller than the data of Henke *et al.* by about 8%. This difference is constant in the wavelength range from 0.6 to 1.8 nm. The most probable explanation is a slightly different structure model for both data sets.

An approximate theoretical value for the intrinsic spectral resolving power of the crystal $(\lambda/\Delta\lambda)_\mathrm{c}$ can be obtained from the differential of the Bragg equation

$$\left(\frac{\lambda}{\Delta\lambda}\right)_\mathrm{c} = \frac{\tan\theta_\mathrm{B}}{\Delta\theta_\mathrm{c}} \tag{3}$$

where $\Delta\theta_\mathrm{c}$ is the FWHM of the reflection curve. This upper limit can not be achieved in practice; an extended source and the typical aberrations of the spectrometer geometry [2–4] cause a broadening. The effect of these geometric factors on the spectral and the spatial resolving power can be taken into account by raytracing calculations (see for example [14]). Unfortunately many of these codes neglect the real reflection properties of the crystals, that is the integrated reflectivity R_int in a first approximation and the reflection curve shape for more precise modelling. These reflection properties can change significantly for bent crystals [5, 15]. Therefore the analysis given here is intentionally limited to a study of the intrinsic X-ray reflection properties of perfect and deformed (mosaic structure, bending) crystals.

A crystal is assumed to be "perfect" if the reflection properties correspond to the results of the dynamical theory of X-ray diffraction. In this case $\Delta\theta_\mathrm{c}$ in eq. (3) can be approximated by the narrow FWHM $\Delta\theta_\mathrm{cp}$ of the reflection curve of a perfect crystal. The corresponding $(\lambda/\Delta\lambda)_\mathrm{cp}$ represents the upper limit for the spectral resolving power of the spectrometer. Unfortunately the real structure of muscovite is not "perfect". X-ray topographic and diffractometric measurements reveal a mosaic structure (see Chap. 4), which broadens the reflection curve. This broadening can be approximated numerically by a convolution of the reflection curve of the perfect crystal with the mosaic spread function (FWHM $\Delta\theta_\mathrm{cm}$). A typical value of $\Delta\theta_\mathrm{cm}$ for muscovite samples with a high degree of perfection is 1 arcmin or 0.017°, respectively (see Chap. 4). In contrast to $\Delta\theta_\mathrm{cp}$, $\Delta\theta_\mathrm{cm}$ is independent of the reflection order l and can be significantly larger than $\Delta\theta_\mathrm{cp}$ for high order reflections. An approximate value of the spectral resolving power $(\lambda/\Delta\lambda)_\mathrm{cm}$ in the mosaic crystal limit can be obtained by replacing $\Delta\theta_\mathrm{c}$ by $\Delta\theta_\mathrm{cm}$ in eq. (3).

A first set of calculations was performed to investigate the reflection properties of flat muscovite crystals in different reflection orders at constant Bragg angles θ_B (50°, 60°, 70°, 80° and 89°). The basic wavelength for each θ_B in the reflection 002 was determined by assuming $d = 2.0047$ nm [10]. For higher reflection orders 00l the corresponding multiples (higher harmonics) of this basic wavelength were used. In Table I the integrated reflectivity R_int, the FWHM $\Delta\theta_\mathrm{cp}$ and the spectral resolving power $(\lambda/\Delta\lambda)_\mathrm{c}$ for selected reflection orders l (reflection 00l) are shown. Reflections with odd numbers l are "forbidden" due to the crystal symmetry. R_int and the FWHM $\Delta\theta_\mathrm{cp}$ for all available reflection orders from $l = 2$ to $l = 24$ are presented in Fig. 1 and Fig. 2, respectively. These data illustrate typical and unique characteristics of muscovite which are important for an experimental application in X-ray spectroscopy and for the quantitative analysis of the measured spectra.

Table I. *Reflection properties (peak reflectivity P, integrated reflectivity R_{int}, FWHM $\Delta\theta_{cp}$ and intrinsic spectral resolution $(\lambda/\Delta\lambda)_c$) of flat muscovite crystals in different reflection orders at fixed Bragg angles θ_B. The basic wavelength λ_0 is selected according to the predefined Bragg angle. The spectral resolving power $(\lambda/\Delta\lambda)_c$ is calculated taking into account a mosaic spread $\Delta\theta_{cm} = 1$ arcmin.*

reflection	002	004	006	00 10	00 16	00 24
($\theta_B = 50°$, $\lambda_0 = 1.52728$ nm)						
P	0.011	0.09	0.24	0.42	0.50	0.51
R_{int} [μrad]	13.7	14.6	29.8	20.0	5.2	1.2
$\Delta\theta_{cp}$ [arcsec]	166	24.8	20.0	8.6	2.0	0.4
$(\lambda/\Delta\lambda)_c$	1480			4000		
reflection	002	004	006	00 10	00 16	00 24
($\theta_B = 60°$, $\lambda_0 = 1.72661$ nm)						
P	0.009	0.15	0.25	0.59	0.62	0.63
R_{int} [μrad]	18.7	33.4	44.6	35.8	9.0	2.1
$\Delta\theta_{cp}$ [arcsec]	288	33.6	27.4	10.6	2.6	0.6
$(\lambda/\Delta\lambda)_c$	1200			5900		
reflection	002	004	006	00 10	00 16	00 24
($\theta_B = 70°$, $\lambda_0 = 1.87348$ nm)						
P	0.009	0.15	0.26	0.62	0.66	0.65
R_{int} [μrad]	31.1	56.5	76	70.1	16.8	3.9
$\Delta\theta_{cp}$ [arcsec]	510	57.0	43.9	19.0	4.4	1.0
$(\lambda/\Delta\lambda)_c$	1100			9400		
reflection	002	004	006	00 10	00 16	00 24
($\theta_B = 80°$, $\lambda_0 = 1.96343$ nm)						
P	0.008	0.15	0.26	0.63	0.68	0.67
R_{int} [μrad]	63.3	128.1	164.5	160.9	38.5	8.8
$\Delta\theta_{cp}$ [arcsec]	1137	126	91.9	42.4	9.6	2.2
$(\lambda/\Delta\lambda)_c$	1000	9000	12000		19000	
reflection	002	004	006	00 10	00 16	00 24
($\theta_B = 89°$, $\lambda_0 = 1.99341$ nm)						
P	0.008	0.15	0.26	0.64	0.69	0.67
R_{int}[μrad]	631.4	1331.8	160.3	1682.5	403.3	92.6
$\Delta\theta_{cp}$ [arcsec]	11708	1308	913	442	99.2	23.4
$(\lambda/\Delta\lambda)_c$	1000	9000	12900	26000	119000	190000

The dependence of R_{int} from the reflection order l (Fig. 1) differs significantly from the behavior of other "standard" analyzer crystals (silicon, germanium and quartz). Typically the integrated reflectivity has its maximum at the first order reflection and decreases for higher orders in correspondence to the decrease of the atomic scattering factor. For muscovite such continuous behavior is not observed. The most intense reflections are $l = 6$ and $l = 10$. For $l = 12$ and 18 the reflections are very weak, but other intense reflections can be observed for higher orders $l = 14$, 16, 20 and 22. Consequently the application of high order reflections is not necessarily connected with a significant loss of luminosity. This is a positive effect which introduces an additional degree of freedom for the optimal experimental setup. Higher reflection orders l with Bragg angles near 90° (see eq. (3)) can be selected to preserve a high spectral resolving power without significant losses of intensity. But on the other hand the observed dependence $R_{int} = f(l)$ indicates that the spectrometer throughput for multiples of the observation wavelength can be considerable due to intense high-order reflections (00l). This additional intensity is recorded at the same Bragg angle, i.e. at the same detector position as the observed spectral line. This will result in

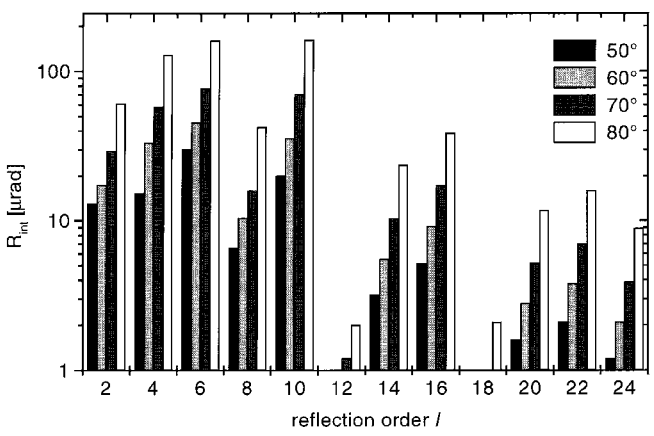

Fig. 1. Integrated reflectivity R_{int} of flat muscovite crystals in the reflection orders 00l ($l = 2 - 24$) at constant Bragg angle (see Table I).

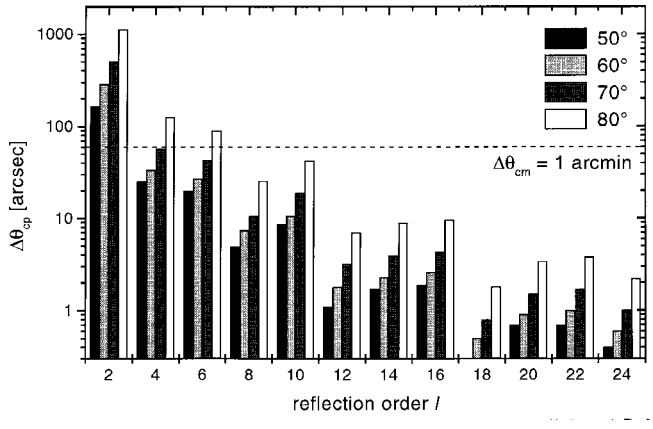

Fig. 2. Full width at half maximum (FWHM) $\Delta\theta_{cp}$ of reflection curves of flat muscovite crystals in the reflection orders 00l ($l = 2 - 24$) at constant Bragg angles (see Table I).

incorrectly determined line intensity ratios, which are often used to determine plasma parameters [16].

The FWHM (cf. Fig. 2) decreases nearly continuously for high order reflections, indicating an increase of the spectral resolving power. The corresponding $(\lambda/\Delta\lambda)_c$ (assuming a mosaic spread $\Delta\theta_{cm} = 1$ arcmin) is shown in Table I. For low order reflections $(\lambda/\Delta\lambda)_c$ is limited by the broad reflections curve and corresponds nearly to $(\lambda/\Delta\lambda)_{cp}$. Theoretically the resolving power $(\lambda/\Delta\lambda)_{cp}$ can reach impressive values of more than 10^5 for high order reflections but in this case the achievable intrinsic spectral resolving power $(\lambda/\Delta\lambda)_c$ is usually limited by the mosaicity, i.e. $\Delta\theta_{cm}$. The optimal region of application for muscovite is the wavelength range $\geqslant 1$ nm. In the wavelength range up to about 0.85 nm the integrated reflectivity for silicon, germanium and quartz is comparable or larger than for muscovite. Furthermore the structure of these crystals is "perfect" and no mosaicity effects have to be taken into account.

Another series of calculations was performed to illustrate the effect of bending on the reflection properties and reflection curve of muscovite. The peak reflectivity P, the integrated reflectivity R_{int}, the FWHM $\Delta\theta_c$ of the reflection curves and the intrinsic spectral resolving powers $(\lambda/\Delta\lambda)_{cp}$ and $(\lambda/\Delta\lambda)_{cm}$ (for a mosaic spread $\Delta\theta_{cm} = 1$ arcmin) were calculated for flat and spherically bent crystals (curvature radii $R = R_x = R_y = 186$ mm or 100 mm, correspondingly) in the reflection orders $l = 2, 4, 6, 10, 16, 24$ for a basic wavelength $\lambda = 1.8602$ nm (reflection 002) and their multiples in the higher reflection orders. The Bragg angle was always fixed to 68.91°. Results are presented in Table II. Obviously the intensity gain for bent crystals due to the crystal deformation (this should not be confused with the intensity gain due to the focusing geometry!) is negligible for low order reflections, but in contrast it can reach a factor of two or more for high-order reflections or a smaller bending radius. The cause is the asymmetric broadening of the reflection curve due to bending which is connected with a decrease of the spectral resolving power for high reflection orders, i.e. short wavelengths. But the main limit for the maximum resolving power is the mosaicity of the mica crystals. This limits $(\lambda/\Delta\lambda)_c$ to $(\lambda/\Delta\lambda)_{cm} \leqslant 8900$ for reflection orders $l \geqslant 4$, which is considerably smaller than the theoretically possible $(\lambda/\Delta\lambda)_{cp}$ for a perfect crystal (Table II).

Typical examples of the reflection curves of flat and bent crystals are shown in Fig. 3 and 4, respectively. For flat crystals the FWHM of the reflection curves decreases for higher reflection orders l, the peak reflectivity increases slightly but the integrated reflectivity decreases (see Table I). The differences between flat and bent crystals are small for low order reflections but become obvious for higher orders. In the reflection 00 16 the reflection curve of the bent crystal (Fig. 4) shows the characteristic oscillating tail for a bent crystal [9], a significantly higher R_{int} and a lower peak reflectivity P than the corresponding reflection curve of the

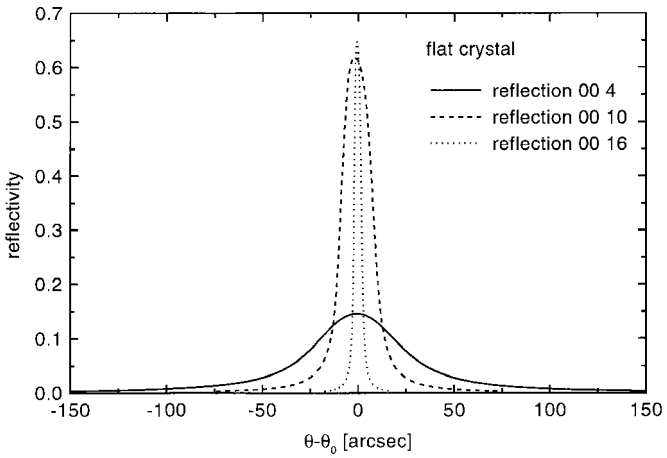

Fig. 3. Calculated reflection curves for flat muscovite crystals in the reflections 004, 00 10 and 00 16.

Table II. *Peak reflectivity P, integrated reflectivity R_{int},* FWHM $\Delta\theta_c$ *and intrinsic spectral resolving powers $(\lambda/\Delta\lambda)_{cp}$ and $(\lambda/\Delta\lambda)_{cm}$ of flat and spherically bent crystals for $\theta_B = 68.91°$ (basic wavelength $\lambda_0 = 1.8602$ nm in the reflection 002) in reflections 002 to 00 24. Obviously the resolving power for high order reflections is limited by the mosaicity ($\Delta\theta_{cm} = 1$ arcmin) and the theoretical values $(\lambda/\Delta\lambda)_{cp}$ given in brackets cannot be achieved in practice*

reflection (flat)	002	004	006	00 10	00 16	00 24
P	0.009	0.15	0.26	0.62	0.65	0.65
R_{int} [μrad]	29	53	71	65	16	3.6
$\Delta\theta_{cp}$ [arcsec]	479	53.4	41.4	17.7	4.1	0.9
$(\lambda/\Delta\lambda)_{cp}$	1100	(10000)	(12900)	(30000)	(>30000)	(>30000)
$(\lambda/\Delta\lambda)_{cm}$				8900		
reflection (sph., $R = 186$ mm)	002	004	006	00 10	00 16	00 24
P	0.009	0.14	0.26	0.60	0.32	0.05
R_{int} [μrad]	28.9	53.6	84.6	66.1	23.4	7.4
$\Delta\theta_c$ [arcsec]	479	50.7	45.6	19.2	8.2	19.9
$(\lambda/\Delta\lambda)_{cp}$	1100	(10500)	(11700)	(27800)	(>30000)	(27500)
$(\lambda/\Delta\lambda)_{cm}$				8900		
reflection (sph., $R = 100$ mm)	002	004	006	0010	0016	0024
P	0.009	0.14	0.26	0.56	0.22	0.03
R_{int} [μrad]	29	53.3	84.2	69.0	26.1	7.6
$\Delta\theta_c$ [arcsec]	479	52.6	46.8	20.6	16.8	33.7
$(\lambda/\Delta\lambda)_{cp}$	1100	(10200)	(11400)	(26000)	(>30000)	(15800)
$(\lambda/\Delta\lambda)_{cm}$				8900		

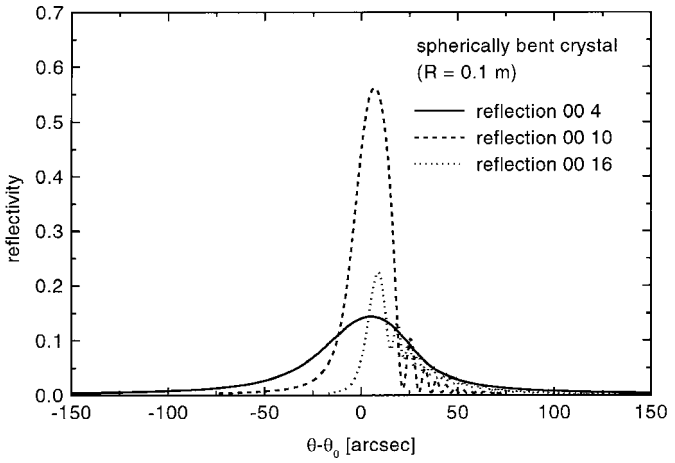

Fig. 4. Calculated reflection curves for spherically bent muscovite crystals ($R = 0.1$ m, reflections 004, 00 10 and 00 16, respectively).

flat crystal. This occurs because the X-ray diffraction from the crystals is more sensitive to the bending deformation for high reflection orders. Crystal bending generally causes the integrated reflectivity to rise from the dynamical (perfect crystal) limit to the kinematical (mosaic crystal) limit [9]. The greater the difference between these two values the larger the luminosity gain can be.

Experimentally determined values of the spectral resolving power, obtained with laser-produced and X-pinch plasmas are in good agreement with the theoretical calculations. Figure 5 and 6 show photographic images and densitograms of X-ray spectra obtained in the reflections 002 and 004 using spectrographs with a spherically bent muscovite crystal. In the spectral range between 1.5 and 2.0 nm (reflection 002) a resolving power $(\lambda/\Delta\lambda)_c > 1000$ can be achieved theoretically (see Table II). This prediction is in good agreement with the experimental values $(\lambda/\Delta\lambda) \sim 730$ for He-like lines of F VIII (Fig. 5). The spectrum was obtained focusing the output of a Nd-glass laser (energy 15 J, pulse duration 2 ns) to a flat CF_2-target. The spot size was about 100 μm. The spherically bent muscovite crystal ($R = 100$ mm, reflection 002, $\theta_B = 57.4°$) was placed on the Rowland circle. A demagnifying geometry is realized: the

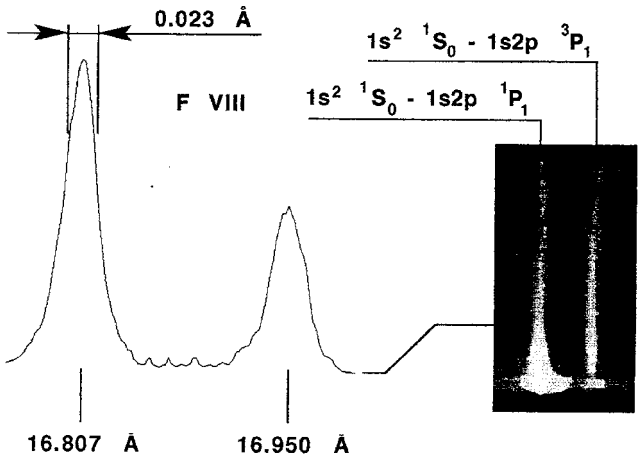

Fig. 5. Spectrum and densitogram of He-like fluorine, obtained from a laser-produced plasma using a spherically bent muscovite crystal ($R = 100$ mm, reflection 002) from a CF_2 target. The spectra were obtained with a single shot of a Nd glass laser (energy 15 J, pulse duration 2 ns).

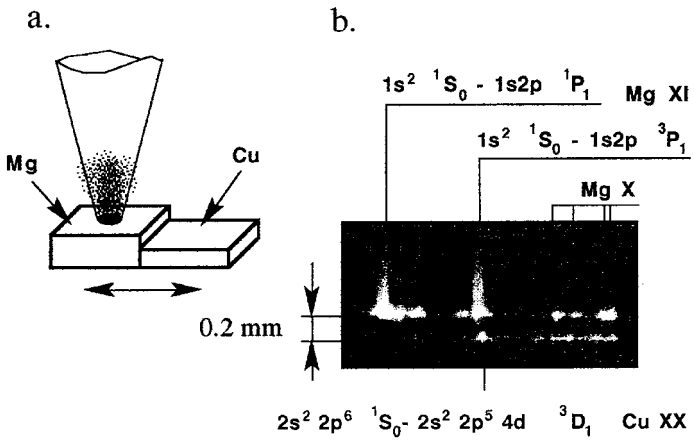

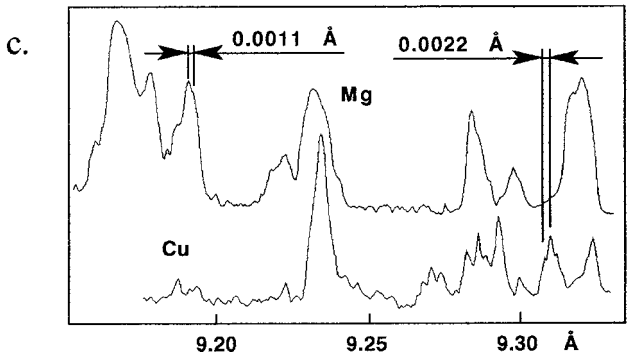

Fig. 6. Results of line coincidence measurements between He-like ions of Mg XI and Ne-like ions of Cu XX. (a) target structure, (b) intensity distribution on the film and (c) photometer scan of the spectrum, obtained with a spherically bent muscovite crystal ($R = 250$ mm, reflection 004). The spectra were obtained with a single shot of Nd-glass laser (energy 15 J, pulse duration 2 ns).

distance crystal-source is 200.6 mm, the distance crystal-film 84.3 mm.

The application of high reflection orders near normal incidence conditions allows highly resolved satellite spectra to be obtained near the resonance lines of He-like ions of Mg XI (Fig. 6) and weak Na-like satellites near 4-2 transitions of Ne-like ions of Cu XX. For this experiment the Nd-glass laser (parameters as above) was focused alternately to a Mg- and a Cu-target (see Fig. 6a for the target shape). The distance between the Mg and Cu surfaces was about 0.2 mm. The spherically bent muscovite crystal ($R = 250$ mm, reflection 004, $\theta_B = 68°$) was placed on the Rowland circle. The distances source-crystal and crystal-film were 321.7 mm and 231.9 mm, respectively. The image is shown in Fig. 6b. A spectral resolving power $(\lambda/\Delta\lambda)$ between 4200 and 8300 can be estimated from the densitogram (Fig. 6c). These values are also in good agreement with value $(\lambda/\Delta\lambda)_{cm} \leqslant 8900$ predicted by Table II for the reflection 004 taking into account a mosaic spread $\Delta\theta_{cm} = 1$ arcmin. All presented spectra in Fig. 5 and 6 were recorded in single shot experiments.

3. Measurements of the integrated reflectivity of flat muscovite crystals

The integrated reflectivity R_{int} of a flat muscovite crystal (thickness 30 μm) was measured with Cu Kα-

($\lambda = 0.154056$ nm) and Mo Kα- ($\lambda = 0.07093$ nm) radiation from conventional X-ray tubes. The geometry of the experimental setup is shown in Fig. 7. R_{int} is low for the investigated high order reflections ($l = 10 - 24$) at these wavelengths. An optimized (n, $+n$) setup [15] with a flat quartz monochromator (reflection $10\bar{1}\bar{1}$) was used to provide high incident intensity on the muscovite crystal.

The X-ray spot at the crystal had a width of about 1 mm in the plane of incidence and a height of 2 mm for Cu Kα and 0.2 mm for Mo Kα radiation. For each reflection order l the distribution of the diffracted intensity near a Bragg peak (angular range $\theta_B \pm \Delta\theta$) was scanned. The integrated reflectivity is determined by the ratio of the angular integrated $I(\theta)$ and the incident intensity I_0,

$$R_{int} = \frac{1}{I_0} \int_{\theta B - \Delta\theta}^{\theta_B + \Delta\theta} I \, d\theta. \quad (4)$$

The results are presented in Table III. The experimental results support the theoretical predictions for the existence of relative intense high reflection orders for muscovite. Such crystals still can be used in reflection orders larger than 10 without a serious loss of luminosity. Error estimates and theoretical values for the integrated reflectivities of perfect (dynamical limit) and mosaic (kinematical limit) crystals are given for comparison. The accuracy of the experimental data decreases rapidly for high order reflections due to low count rates. Neglecting the data with largest errors at the highest reflection orders, the measured integrated reflectivities are between the dynamical and the kinematical limit. This corresponds to the predictions that mosaicity causes R_{int} to rise from the dynamical to the kinematical limit. Consequently, the degree of perfection of the measured crystal is intermediate between perfect and mosaic crystal. Quantitative values for the degree of crystal perfection are achieved using X-ray topography, for example.

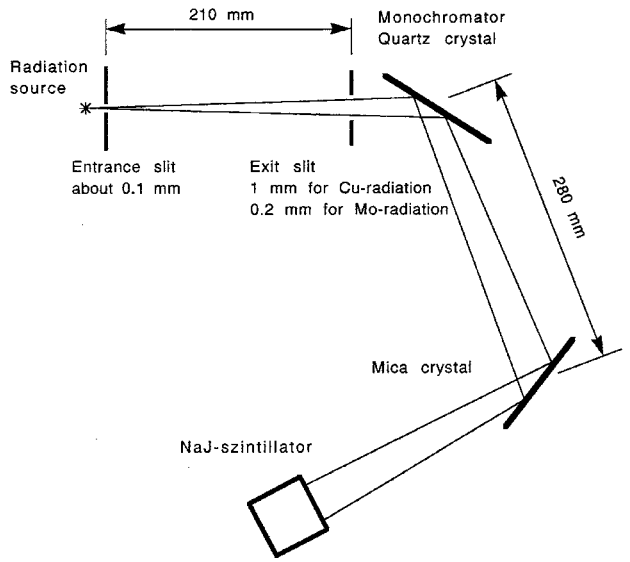

Fig. 7. Experimental set-up for the measurement of the integrated reflectivity R_{int} of flat muscovite crystals.

4. Topographic studies of the crystallographic perfection of flat and spherically bent crystals

Practical experience shows that the crystallographic perfection of large natural muscovite crystals can differ considerably between different samples. Thus it is essential to select a high-quality specimen before bending. It is just as essential to check the samples already bent. Standard test methods for the perfection of large crystals are measurements of the angular shifts and/or deformations of the single crystal rocking curves inside selected crystal areas and x-ray projection topography [17]. Both test methods have been modified for the investigation of bent crystals and schemes are presented in Fig. 8.

Large crystal areas can be characterized by scanning of the sample (along of the coordinate x) in front of the X-ray beam (see Fig. 8). The following conditions determine the adjustment of the goniometer:

1. The goniometer axis is perpendicular to the diffraction plane of the X-rays
2. The crystal surface and the X-ray beam are centred to the goniometer axis.

The absolute angular position $\alpha_{th}(x)$ of the goniometer corresponds to the calculated Bragg position at a given position x. For flat crystals α_{th} is independent of the coordinate x. For bent crystals the adjustment changes during the scan due to the curvature of the lattice planes. A readjustment is realized by an additional translation $y(x)$ to move the crystal surface back to the gonoimeter axis and a rotation to $\alpha_{th}(x)$. Both values are calculated using the given radius of curvature R_x in the diffraction plane. Due to misorientations (tilts, different lattice plane distances and errors of the curvature radius) between crystal areas the experimentally determined Bragg position $\alpha_{exp}(x)$ can be different

Table III. *Measured data, dynamical and kinematical limits of the integrated reflectivity for CuKα- and MoKα-radiation*

	R_{int}(Cu Kα_1) [μrad]			R_{int}(Mo Kα_1) [μrad]		
reflection	exp.	dyn. limit	kinemat. limit	exp.	dyn. limit	kinemat. limit
00 10	25.4 ± 1.0	14.7	77.9	33.6 ± 0.70	8.0	191.4
00 12	1.5 ± 0.1	0.8	1.1	1.3 ± 0.05	0.8	2.9
00 14	3.9 ± 0.1	2.6	6.1	4.6 ± 0.14	1.9	16.3
00 16	5.1 ± 0.1	4.0	13.7	0.69 ± 0.02	2.7	36.8
00 18	0.3 ± 0.03	0.3	0.3	0.25 ± 0.02	0.3	0.9
00 20	2.0 ± 0.1	1.7	3.7	1.5 ± 0.06	1.1	7.7
00 22	4.3 ± 0.2	3.4	8.8	2.2 ± 0.07	1.3	12.5
00 24	3.1 ± 0.2	3.5	7.2	1.0 ± 0.04	0.83	5.6
00 26				0.84 ± 0.05	0.83	6.1

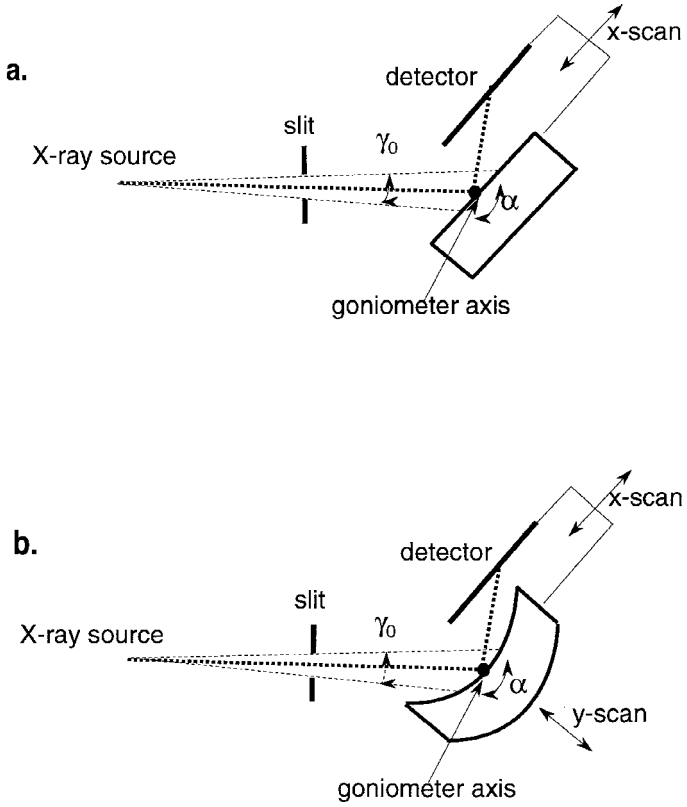

Fig. 8. Scheme for measurements of crystal rocking curves and projection topographs of flat (a) and bent (b) crystals.

from $\alpha_{th}(x)$ and the angular shift of the single crystal rocking curve $\Delta\alpha(x) = \alpha_{th}(x) - \alpha_{exp}(x)$ characterizes the amount of these misorientations.

The size of crystal areas with misorientations smaller than an angle γ can be determined with projection topography. The angle γ is experimentally fixed by the horizontal divergence of the incoming beam γ_0 and also by the bending radius. The thickness of the surface layer analysed is determined by the penetration depth of the X-rays which is limited by the absorption depth (35 μm) for an ideal mosaic crystal and the extinction depth (9.3 μm) for a perfect crystal, respectively. It varies between both limits according to the local perfection. Typical results for flat and spherically bent ($R = 100$ mm) muscovite crystals (size $30 \times 10\,mm^2$, thickness 100 μm) with a high degree of perfection are shown in Fig. 9 and 10, respectively using Cu $K\alpha_1$-radiation (reflection 00 22, $\theta_B = 58.2°$). For perfect crystals a nearly constant optical density over the whole crystal area should be visible in the topograph; in fact the topographs of the muscovite crystals (Fig. 9a and 10a) show obvious local density variations. The local misorientation exceeds γ (Fig. 9a: $\gamma = \pm 6$ arcmin, Fig. 10a: $\gamma = \pm 7.5$ arcmin) at the edges of the crystals and the optical density of the topograph goes to zero. Additionally extinction contrast is visible, which is caused by grain boundaries or bending defects.

To obtain a quantitative information about the misorientation the angular shifts $\Delta\alpha(x)$ of single crystal rocking curves are shown in Fig. 9b and Fig 10b for the flat and bent crystal, respectively. The scan for the flat crystal shows a superposition of a long-range deformation (the continuous increase of $\Delta\alpha(x)$ in Fig. 9a) with some fluctuations. Where the fluctuations are obviously connected with different

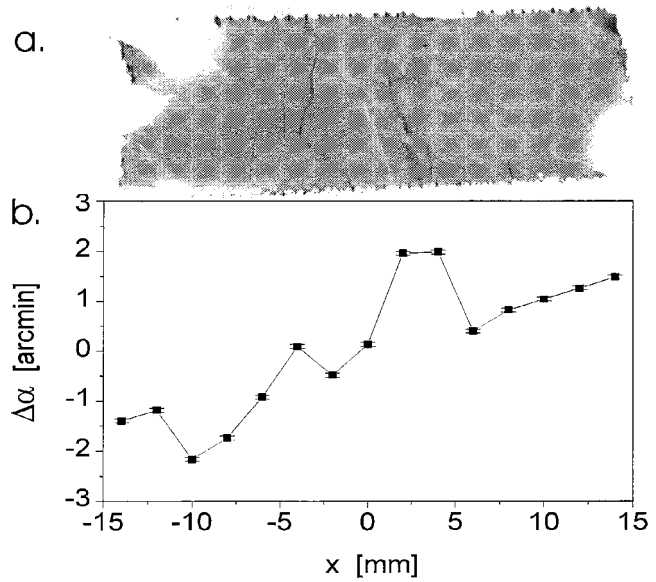

Fig. 9. Projection topograph (a) and angular shift of single crystal rocking curves $\Delta\alpha(x)$ as a function of the scan position x along the center line (b) of a flat muscovite crystal (size $30 \times 10\,mm^2$, $CuK\alpha_1$-radiation, reflection 00 22). The spot size for the rocking curve measurement was $0.25 \times 1\,mm^2$.

(tilted to each other) grains (compare Fig. 9a and 9b), the long-range deformation cannot be ascribed to a single cause. Possible origins can be curvatures of the thin crystal due to internal stresses or deformations due to the crystal mounting. A separation of these two factors is not possible. A linear fit of $\Delta\alpha(x)$ shows that the standard deviation due to the misorientation fluctuations is less then 1 arcmin for the flat crystal. For the spherically bent crystal the error bars are larger and are caused mainly due to the lower accuracy of adjustment. The deformations are largest at the edges of the crystal. A linear fit of the data points neglecting the edges gives a standard deviation of about 1.5 arcmin.

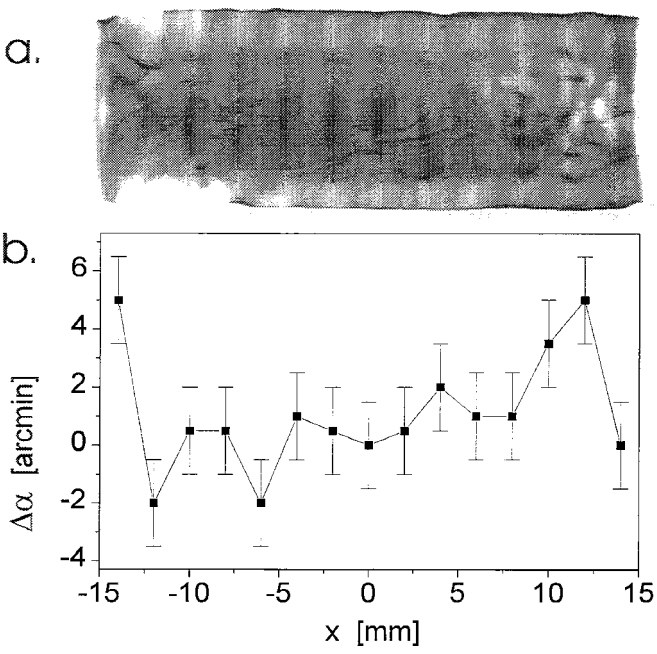

Fig. 10. Projection topograph (a) and angular shift of single crystal rocking curves $\Delta\alpha(x)$ as a function of the scan position x along the center line (b) of a spherically bent muscovite crystal ($R = 100$ mm, size $30 \times 10\,mm^2$, $CuK\alpha_1$-radiation, reflection 00 22). The spot size for the rocking curve measurement was $0.25 \times 1\,mm^2$.

In conclusion this study once more underlines the need to test the crystallographic perfection of the muscovite samples even before preparation. It also shows that bent muscovite crystals can be prepared with small radii of curvature without introducing significant additional defects. For samples with the best quality (cfg. Fig. 9) the deformations due to mosaicity, internal stresses (and bending effects) do not exceed about 6 arcmin over the whole sample. For small crystal areas of such samples (some mm^2) a mosaic spread of 1 arcmin is representative.

5. Test of the imaging properties of spherically bent crystals

A test of the imaging properties of spherically bent muscovite crystals in the same wavelengths range as in the experiments is carried out with different plasma sources (laser-produced plasma or x-pinch plasma [18]). For an imaging test with a laser produced plasma (see Fig. 11) the source (1) is placed at the Rowland circle (6) at a distance of 99.8 mm from the crystal. A mesh (3) is positioned inside the Rowland circle at the distance $a = 66.7$ mm from the crystal. This distance is chosen according to the focal equation for a spherical mirror: $1/a + 1/b = 2/R$. The detector (photographic film) is placed at the distance $b = 199.98$ mm from the crystal ($R = 100$ mm, reflection 006, $\theta_B = 86.3°$, size $30 \times 10\,mm^2$). A Nd-glass laser (energy 15 J, pulse duration 2 ns) was focused to the surface of an Al target and the mesh and crystal were illuminated with the intense He-line of Al XII ($\lambda = 0.66343$ nm). The total image size on the film was about $10 \times 5\,mm^2$ (Fig. 11b), which corresponds to a magnification M of about three. The individual wires of the mesh (diameter 25 μm) were clearly resolved inside the whole imaged area. According to the scan (Fig. 11b) the edge spread of the wire image was about $\delta = 10$ μm and δ allows an estimate of the average misorientation (including mosaic spread and bending geometry errors) of the bent crystal. It should be about $\Delta\theta = M\delta/[(1 + M)R] \approx 0.8 \cdot 10^{-4} \approx 0.3$ arcmin. Additional experiments, using a x-pinch as a brighter X-ray source (see Fig. 11c) and a higher magnification of 5 showed that a spatial resolution better than 4 μm can be achieved. The glass fiber (diameter 8 μm) in Fig. 11c is clearly resolved. Under these conditions the average misorientation of this crystal specimen should be smaller than $\sim 0.4 \cdot 10^{-4}$ rad or 0.15 arcmin, at least in the area of $2 \times 2\,mm^2$, which was used for the imaging.

6. Summary

We present theoretical and experimental data to characterize the reflection properties of flat and bent muscovite crystals. Due to the large lattice parameter muscovite can be used in the wavelength range $\geqslant 1$ nm where only a few crystals are available. Calculations of the reflection properties show some properties which are unique for muscovite, in particular the existence of intense high-order reflections. Possible experimental consequences are discussed.

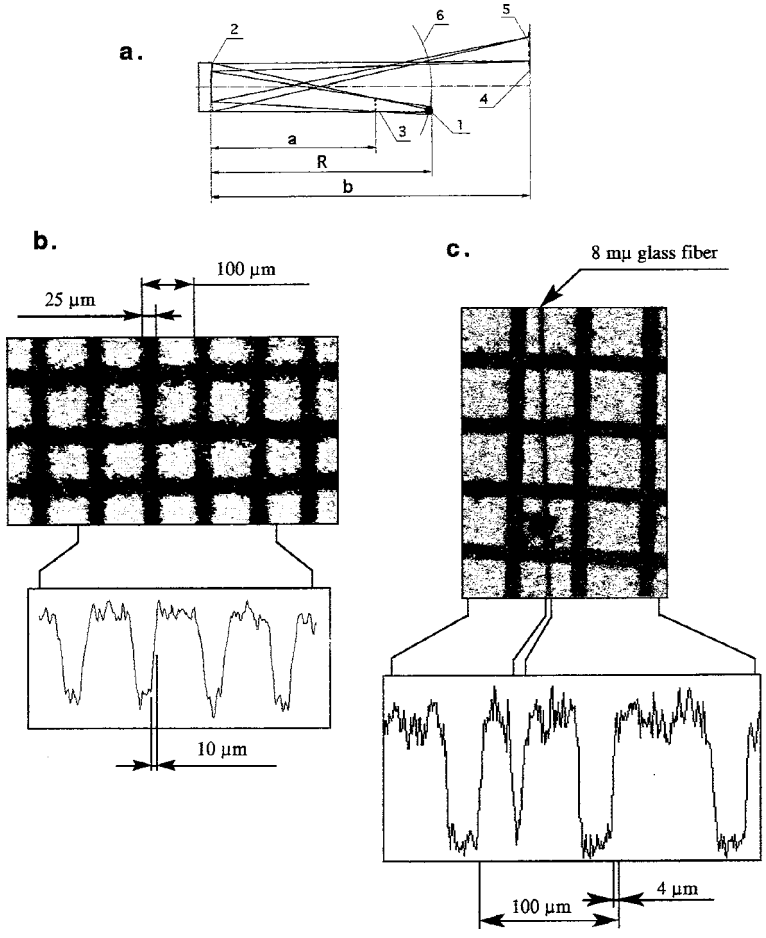

Fig. 11. Test of the imaging properties of a spherically bent muscovite crystal ($R = 100$ mm, reflection 006): (a) scheme (1-plasma source, 2-spherically bent crystal, 3-test mesh, 4-film, 5-image of test mesh, 6-Rowland circle); (b) mesh image, obtained with a laser plasma source and the corresponding photometer scan; (c) mesh image, obtained with a x-pinch plasma and the corresponding photometer scan.

X-ray topography and diffractometric measurements reveal a mosaic structure of the muscovite samples. They can have a high degree of crystal perfection (mosaic spread $\Delta\theta_{cm} \approx 1$ arcmin). This mosaicity limits the spectral resolving power, especially for high-order reflections, i.e. for short wavelengths. The advantages of muscovite are most apparent in the long wavelength range $\geqslant 1$ nm.

Furthermore the presented results show that the muscovite samples must be carefully preselected already before preparation (bending) and use to obtain crystals with a high crystal perfection, i.e. with a small mosaic spread. The experimental results for bent samples show also the high standard of the preparation technology for spherically bent crystals. Such bent muscovite crystals were used for a large number of applications, such as highly precise wavelength measurements [19–21] coincidence measurements of different spectral lines pairs [22–24], diagnostics of plasma [20, 25–28] in a wide spectral range from 0.11 to 1.9 nm.

Acknowledgements

This work was partly supported by Russian Fundamental Science Foundation Grant 96-02-15410. The authors would like to thank Dr. R. J. Hutcheon for assistance in preparing the text.

References

1. Burek, A., Space Science Instrum. **2**, 53 (1976).
2. Johann, H. H., Z. Physik **69**, 185 (1931).
3. Johansson, T., Z. Physik **82**, 507 (1933).
4. Hamos, L. v., Z. Kristallog. **101**, 17 (1939).
5. White, J. E., J. Appl. Phys. **21**, 855 (1950).
6. Förster, E., Gäbel, K. and Uschmann, I., Laser Particle Beams **9**, 135 (1991).
7. Förster, E. *et al.*, J. Quant. Spectrosc. Radiat. Transfer **51**, 101 (1994).
8. Deutsch, M. *et al.*, Phys. Rev. **A51**, 283 (1995).
9. Taupin, D., Bull. Soc. franç. Minér. Crist. **87**, 469 (1964).
10. Güven, N., Z. Krist. **134**, 196 (1971).
11. Pinsker, Z. G., "Dynamical Scattering of X-Rays in Crystals," (Springer-Verlag, Berlin/Heidelberg/New York 1978).
12. Landolt-Börnstein "Numerical Data and Functional relationships in Science and Technology" (Ed. K.-H. Hellwege), New Series/Group III/Volume 11, (Springer-Verlag, Berlin/Heidelberg/New York 1979).
13. Henke, B., Gullikson, E. and Davies, J., Atomic Data Nucl. Data Tables **54**, 181 (1993).
14. Dirksmöller, M. *et al.*, Opt. Comm. **118**, 379 (1995).
15. Uschmann, I., Förster, E., Gäbel, K., Hölzer, G. and Ensslen, M., J. Appl. Cryst. **26**, 405 (1993).
16. De Michelis C. and Mattioli, M., Nucl. Fusion **21**, 677 (1981)
17. Dressler, L., Kafka, F., Kräusslich, J. and Wehrhan, O., Cryst. Res. Technol. **25**, 1097 (1990).
18. Pikuz, S. A., *et al.*, JETP Lett. **61**, 638 (1985).
19. Khakhalin, S. Y. *et al.*, Physica Scripta **50**, 106 (1994).
20. Bryunetkin, B. A. *et al.*, J. Quant. Spectrosc. Radiat. Transf. **53**, 45 (1995).
21. Bollanti, S. *et al.*, Physica Scripta **51**, 326 (1995).
22. Bryunetkin, B. A., Dyakin, V. M. and Nilsen, J., Quantum Electron. **24**, 133 (1994).
23. Nilsen, J. *et al.*, Phys. Rev. **A50**, 2143 (1994).
24. Faenov, A. Y. *et al.*, Phys. Rev. **A52**, 3644 (1995).
25. Bryunetkin, B. A. *et al.*, Quantum Electron. **23**, 337 (1993).
26. Pikuz, S. A. *et al.*, J. Quant. Spectrosc. Radiat. Transf. **51**, 291 (1994).
27. Bartnik, A. *et al.*, Quantum Electron. **25**, 50 (1995).
28. Faenov, A. Y. *et al.*, Phys. Rev. **A51**, 3529 (1995).